ABL-Based Thermoplastic Rubber Adhesive for Enhanced Metal-to-Metal Joining

*Zeyang Yu [a], Nihal Kanbargi [a], Sumit Gupta [a], Yongsoon Shin [b], Yao Qiao [b], Christopher C. Bowland [a], Daniel R. Merkel [b], Kevin L. Simmons [b], Amit K. Naskar [a]**

[a]*Oak Ridge National Laboratory, 1 Bethel Valley Rd, Oak Ridge, TN 37830, USA*
[b]*Pacific Northwest National Laboratory, 902 Battelle Blvd, Richland, WA 99352, USA*

**Email: naskarak@ornl.gov*

Abstract

With the growing requirement for lightweight structural materials in automotive, aerospace, and infrastructure applications, multi-material joints made with adhesive have attracted intense research interest. Commercial thermoset adhesives are one-time cures, and difficult to disassemble the bonded components for repair and recycling. Our prior work with a thermoplastic acrylonitrile-butadiene-lignin rubber (ABL) addresses this sustainability/recycling challenge, but the adhesive exhibits deficient joining strength compared to standard thermosets. Here, we modify the ABL matrix by loading particulate fillers to enhance its modulus and toughness. The goal is to manufacture a cure-free thermoplastic adhesive system with a simple dispensing protocol and characteristic ductility combined with a high yield stress for improved shear strength of a bonded joint. Fumed silica (FS) and epoxidized glass spheres (EGS) were used as fillers in the ABL to promote the dispersion of lignin particles that tailored the functionalities and free energy components of the adhesive surface. With optimal loading of FS (5 wt.%) and EGS (30 wt.%) in ABL adhesive matrix, the lap-shear strength of bonded aluminum joint was elevated by 128%, compared to the neat ABL, reaching 21 MPa, which is 90% of the performance of a commercial epoxy-based adhesive.

*Corresponding author: Carbon and Composites group, Oak Ridge National Laboratory, 1 Bethel Valley Rd, Oak Ridge, TN 37830. Email: naskarak@ornl.gov.

This manuscript has been authored by UT-Battelle, LLC, under contract DE-AC05-00OR22725 with the US Department of Energy (DOE). The US Government retains, and the publisher, by accepting the article for publication, acknowledges that the US Government retains a nonexclusive, paid-up, irrevocable, worldwide license to publish or reproduce the published form of this manuscript, or allow others to do so, for US Government purposes. DOE will provide public access to these results of federally sponsored research in accordance with the DOE Public Access Plan (http://energy.gov/downloads/doe-public-access-plan).

For Peer Review

Highlights

- A partly renewable filler-toughened thermoplastic adhesive has been developed.
- This thermoplastic gives nearly equivalent performance of adhesively bonded aluminum joint compared to standard thermosets.
- Experimental and simulation data help understand the adhesive reinforcing mechanism by the fillers.

KEYWORDS: Adhesion, Joints/joining, Lignin.

For Peer Review

1. INTRODUCTION

Adhesively bonded joints are important to enable lightweighting in multi-material automotive components. Adhesives not only bonds various types of metals and lightweight fiber-reinforced composites but also can eliminate fasteners, drilling, and associated stress concentrations in a part. Adhesives spread the load on larger areas and can adhere similar or dissimilar materials. For the hybrid joints, the existence of adhesive layer can improve fatigue strength and furthermore, the adhesive layer can function as the protecting layer for metal substrate from corrosion.[1] However, the joint using the conventional thermoset adhesives cannot be disassembled for maintenance and repair if the curing process is completed. Therefore, developing a thermoplastic adhesive that gives similar or better bonding strength than standard thermoset adhesives offers a promising alternative way to re-assemble or repair the bonded joints.[2] Another inspiration for designing future adhesives is improving the sustainability of adhesive products and their manufacturing processes.[3] From the sustainability point of view, it is necessary to obtain the adhesive production in an environmentally friendly way without negatively affecting the adhesive's properties.[4] Several guiding principles have been posted to direct the adhesive manufacturing in a more sustainable manner: replacement of petroleum-based components with bio-based alternatives, solvent-free formulations, and

replacement of organic solvents.[5] Developing the more sustainable adhesives is a partial way to address all the environmentally related issues. The main challenges to realizing the circular economy and reducing the waste production in adhesive industry is to modify the current status in the areas of the sustainability of raw materials and adhesive product, recovery and recycling after use, and feasibility of reintroducing components into the production flow.[5] To that end, our ongoing work on lignin-based thermoplastics,[6, 7] if useful as adhesive, has potential to improve its sustainability and because of its thermoplastic nature, the bonded joint can be disassembled by heating above the adhesive's glass transition temperature. As the main component of a potential formulation, lignin exists as the second most abundant biopolymer on earth.[8, 9] So far, lignin has been utilized in various applications over the past decades instead of just being taken as the by product in the paper manufacturing industries. Besides being directly used as solid fuels, lignin and its derivatives can be used as the precursors for carbon materials,[10] raw materials to prepare various surfactants,[11] components for energy storage devices,[12] and functional and structural fillers for polymer composites.[13] Naturally, lignin is a crosslinked network of amphiphilic molecules that function as the primary adhesive component to maintain the structural integrity of plant cell walls and in the past a few years, lignin-based adhesives have also been used for substrates such as metals[14] and glass.[15] Furthermore, making use of the biobased materials can reduce carbon dioxide production because of their higher biodegradability compared to the synthetic materials.[16, 17]

Nitrile butadiene rubber (NBR), another main component of adhesive in this research, is commonly used in industrial and automotive areas because of its excellent resistance to lubricants and chemicals, low cost, and its properties can be easily designed by adjusting the acrylonitrile content.[18, 19] However, its mechanical strength is weak without reinforcements. To promote the application performance of NBR, many types of fillers are added to the polymer matrix to improve

For Peer Review

not only its mechanical properties[20] but the electrical conductivity,[21] thermal stability,[22] and fraction and abrasion properties.[23] Furthermore, great efforts have been put into synthesizing the acrylonitrile and butadiene using the biomass.[24, 25]

Inspired by toughness and thermo-mechanical response of lignin-derivative from melt-mixed formulations of lignin and NBR,[7] our recent work investigated utilization of, specifically, technical hardwood organosolv lignin-based thermoplastic as adhesive for joining steel substrates.[26] These works realized that a high polarity nitrile rubber (NBR 51, i.e., NBR with 51 mol% nitrile content) forms stronger and stiffer composition when mixed with melt-processable lignin. Increased rubber matrix polarity enhanced its miscibility with lignin. The thermoplastic composition is termed acrylonitrile-butadiene-lignin resin or abbreviated as ABL. We analyzed the impact of nitrile content in NBR that used in ABL formulation and lignin content in ABL on the adhesion properties and performance of steel joints. Out of all the samples tested, the NBR with 51% acrylonitrile content and 60 wt.% lignin composition had the strongest lap shear strength, which was chosen as the baseline for this research. In our prior investigation, we observed the occurrence of cohesive failure in ABL adhesives during the single lap shear strength test.[26] Cohesive failure in adhesive occurs when the adhesive material itself ruptures or breaks apart rather than separating from the substrate which it was applied to. In other words, cohesive failure happens when the bond between the adhesive and the substrate remains strong, but the adhesive material itself is not strong enough to withstand the forces being applied to it. Therefore, improving the mechanical properties of ABL composites is necessary to augment the adhesive strength of ABL-based adhesives. We hypothesize that incorporating stiff reinforcements into ABL will enhance its mechanical properties, thereby increasing the lap shear strength of ABL-based adhesives. Designing stronger ABL-based adhesive requires a thorough investigation of the underlying mechanisms responsible

For Peer Review

for the reinforcement provided by the fillers and this knowledge can be utilized to inform the development of ABL-based adhesives. Hence, developing a computational framework for ABL-based composites could facilitate the investigation of how integrating nanoparticles into the ABL matrix strengthens its overall mechanical properties through a reinforcing mechanism. However, the computational cost of explicitly modeling nanoparticles in the ABL matrix can be significant. Micromechanics involves the assessment of the global characteristics of heterogeneous materials (*e.g.*, ABL-fumed silica (FS) composites), given that the properties of the individual components and their spatial configuration are known a priori. Here, the representative volume element (RVE) offers a means of addressing heterogeneous materials with nearly homogenous macroscopic structures at a suitable length scale. The nanosized FS can also affect both segmental and chain-scale polymer dynamics due to confinement, which modified the composites' viscoelastic properties, achieving better dispersion and separation of lignin particles during the melt-blending process. The rich hydroxyl groups on FS offer good affinity with ABL matrix and adjust the adhesive surface chemistry. Particles of relatively larger length-scale, epoxy-functionalized glass spheres (EGS) can bring in the ball milling effect during the mixing process, leading to additional optimization on lignin particles separation. Additionally, the epoxy functional groups on EGS are beneficial for improving the surface energy and the wettability of the adhesive. The computational results were compared with the experimental data and the reasons of difference were analyzed. The rheological properties of the ABL-based adhesives were investigated at the end to evaluate their processability.

State-of-the art structural adhesives used in metal-to-metal joining are thermoset polymers with permanent crosslinked network that makes disassembly of parts difficult. This research addresses need for a structural thermoplastic adhesive that can help disengage adhesively bonded joints via

For Peer Review

thermal de-bonding. In this study, we report a thermoplastic adhesive without requiring any crosslinking agent (or curing step) that gives nearly equivalent bonding strength of a standard thermoset adhesives.[27-30] Furthermore, we meet the sustainability need of the thermoplastic adhesive via utilization of a biorefinery and paper or pulping mill coproduct, lignin. Partly renewable filler-toughened thermoplastic adhesive based on ABL composition has been investigated in this work where experimental and simulation data help understand the adhesive reinforcing mechanism. Our newly developed toughened adhesive provides great potential to replace commercial petroleum-based products. Additionally, the processable film or sheet-like structure of the adhesive facilitates its operation, waste minimization, storage, and avoids any 'squeeze out' drawbacks when combined with industrial joining techniques.

2. MATERIALS AND METHODS

2.1 Materials

The nitrile rubber was purchased from Scientific Polymer Inc. The lignol lignin was received from Lignol Innovations LLC, Canada. The fumed silica AEROSIL R202 was purchased from EVONIK Industries. The epoxy functionalized glass spheres E3000 were supplied by Potters Industries. The 0.8 mm thick aluminum 6061 adherent was purchased from McMaster-Carr and cut into 25.4 mm by 101.6 mm for preparing single lap shear test samples.

2.2 Adhesive preparation

All the ABL-based adhesives were prepared through a Brabender internal mixer. NBR 51 and 60 wt.% lignin were shear mixed under 160 °C and 90 rpm for 3 min, then various amounts of FS (2 wt.%, 5 wt.%, 7 wt.%, 10 wt.%) were added into the chamber and the mixing process lasted for 35 min. The produced compounds were labeled as ABL-FS. Selective amounts of EGS (5 wt.%, 15 wt.%, 30 wt.%, and 45 wt.%) were transferred into the chamber after initial shear mixing of

For Peer Review

ABL and FS for 3 min and continued to mix for 35 min to produce ABL-FS-EGS composite adhesives. For the control ABL sample, the NBR 51 and 60 wt.% lignin were shear mixed under the same temperature and rotation speed for 35 min. Neat ABL and its reinforced composites were pressed into films by placing the material between two 254 × 254 mm^2 metal plates covered with Teflon films using a carver press at 180 ºC, 90 kN for 15 min. To control the thickness of produced film (0.35 mm), a frame shim was placed between the plates.

2.3 Single-lap shear (SLS) test sample preparation

The aluminum adherent was polished with 320 grit sandpaper and sonicated in acetone at room temperature for 15 min before use. The above-prepared adhesive films were cut into 12.7 × 25.4 mm^2 rectangular shapes and placed between two Al bars. A schematic illustration of an SLS sample preparation and the fixture is shown in Figure S1. Five duplicates were pressed at 180 ºC and a pressure of 55 MPa for 25 min to obtain the bonded samples. A spacer was used to control the adhesive layer thickness (0.25 mm).

2.4 Adhesive characterization

The adhesive films were cut into Type V dog bones and the tensile properties were tested with an MTS testing system Alliance RT/5 based on the ASTM D638. The testing speed was 50 mm min^{-1}, and the displacement was recorded using an MTS long travel extensometer. The lap shear strength (LSS) was investigated using the same MTS testing system based on the ASTM D3165 with a speed of 1.27 mm min^{-1} and sets of five specimens were tested for each type of adhesive.

The adhesives' Fourier Transform Infrared (FTIR) spectra were collected in attenauted total reflection (ATR) mode with a Perkin Elmer instrument and 128 scans with 4 cm^{-1} resolution were adopted to analyze each adhesive film. Baseline correction was applied. The absorbance of the peak corresponding to the -CN band observed at 2238 cm^{-1} was used to normalize the spectra.

For Peer Review

Surface free energy was measured based on Owens, Wendt, Rabel, and Kaelble (OWRK) method. The contact angles on the sample surfaces were recoreded using KRŰSS Mobile Surface Energy Analyzer (KRŰSS USA, Matthews, NC USA) with two kind of liquids (water and diiodomethane). Each sample was measured by five times to obtain the average value. A detailed process was discussed in our previous manuscript.[31]

The dynamic mechanical properties of the adhesive were analyzed with a TA instrument RSA-G2 solids analyzer. The storage modulus (G') and loss modulus (G") were recorded in the temperature range from -50 to 200 °C with a temperature increasing step of 3 °C min^{-1} and 1 Hz frequency. The mechanical damping factor tan δ was calculated as the ratio of G" and G'.

The rheological properties of the adhesives were investigated by a Discovery Hybrid Rheometer (DHR-3, TA Instruments). The linear region of G' was determined by frequency sweep from 100 to 0.1 rad s^{-1} with a 1% strain amplitude. The rheological properties were then analyzed using strain sweep with an angular speed of 100 rad s^{-1} at 160 °C. The axial force was set as 1 N for the tests with a sensitivity of 0.5 N.

The cryogenically fractured surfaces of the ABL-based adhesive surfaces were investigated with a MIRA3 TESCAN scanning electron microscope (SEM). All of the images were collected with a working distance of 10 mm, with an accelerating voltage of 10 kV.

2.5 Representative volume element (RVE) modeling

To investigate the underlying mechanisms responsible for the reinforcement provided by the fillers and utilize this knowledge to inform the development of ABL-based adhesives, a computational framework was developed for these composites. The representative volume element (RVE) offers a means of addressing heterogeneous materials with homogenous macroscopic structures at a continuum length scale. RVE is a small volume of material that is statistically

For Peer Review

representative of the entire composite.[32] In our particular scenario, ABL-based composites could be simplified as a series of regular microstructures that make up the RVE. By subjecting these RVEs to various loads with relevant boundary conditions and examining their stress-strain behavior through finite element (FE) modeling, we aim to investigate the mechanical properties of the composites. The details about the RVE modeling are included in supporting information (SI).

3. RESULTS AND DISCUSSIONS

3.1 Adhesion of ABL-based adhesive

The RVE analysis was used to facilitate the investigation of how integrating FS nanoparticles into the ABL matrix strengthens its overall mechanical properties through a reinforcing mechanism. However, we found that it is not feasible to generate RVE models with higher weight percentages of nanoparticles beyond 7 wt.%, due to the jamming effect,[33] so Figure 1 included the simulated properties of an ABL-FS composite with FS loading up to 7 wt.%. Figures 1a-1o illustrates the spatial distribution of *X*-component stress (σ_{11}) (the 2D RVE and X, Y axis definition were described in Figure S2) within the RVEs with different *wt*.% of FS at varying ε_{avg} (the average tensile strain in X direction, see equation presented in SI). As the magnitude of ε_{avg} increases from 0% to 2%, there is a gradual shift in color from blue to red that becomes noticeable, indicating more induced stresses within the composites. In these plots, we observed that the stress distributions were non-uniform. The particles experienced high-stress levels, while the ABL matrix underwent less stress, as observed in zoomed-in stress distribution maps (Figures 1e, 1j, and 1o, insets). This result is reasonable, as the highly stiff FS nanoparticles ($E_{FS} \approx 135 \times E_{ABL}$) function as reinforcements and bear most of the stresses within the composites, thereby protecting the ABL matrix from damage. ABL-FS composites' peak stresses were characterized from the computational study. We found that 2, 5, and 7 wt.% FS nanoparticle-based composites have peak

For Peer Review

stress equal to ~16, ~17, and ~17.5 MPa, respectively (Figure 1s). The maps of plastic strain in the *X* direction (PS_{11}) corresponding to the peak stress (Figures 1p-1r) reveal the buildup of plastic deformation inside the RVEs. It was observed that a continuous band formed within the PS_{11} maps of the 2 wt.% composites (Figure 1p), indicating a global failure of the RVE. On the other hand, accumulations of PS_{11} were discrete in the case of 5 and 7 wt.% composites (Figures 1q and 1r, respectively) suggesting the overall strengthening of the composites via FS reinforcement. We hypothesized that stiff FS nanoparticles within the ABL offer a more torturous pathway towards a continuous failure surface formation. When we zoomed in on the PS_{11} plot of 2 wt.% composites (Figure 1p, inset), we found that the deflection of the failure plane from the location of the microparticles validates our hypothesis. Despite the limitations of the proposed RVE modeling technique, this computational study demonstrates that the inclusion of FS nanoparticles in ABL can improve its mechanical properties, which could enhance the adhesion properties of ABL.

Based on the computational data, the mechanical properties of ABL-FS with 2 wt.%, 5 wt.%, and 7 wt.% FS were selected for investigation. ABL with 10 wt.% FS was also prepared to explore the performance of the composite beyond the computational limit. The experimental tensile strength and adhesion of all the ABL-based adhesives were tested and used to compared with the simulated results, which were shown in Figures 1 (t) and (u). With the incorporation of 2 wt.%, 5 wt.%, 7 wt.%, and 10 wt.% FS to the ABL matrix, the tensile strength of composite adhesives was increased by 75%, 93%, 76%, and 54%, respectively. Besides being used as the reinforcing fillers, the FS also worked as the thickening agent that additionally modified the rheological properties of composites during the melt shear mixing process, which helps the separation and dispersion of lignin phase leading to improved tensile strength. Reflected in Figure S4, with the addition of FS, the size of lignin domains decreased, and a more uniform dispersion condition of lignin was

For Peer Review

achieved. However, after 5 wt.% loading, continuously increasing the loading of FS led to a drop in tensile strength, which was caused by the particle aggregation and difficulty of dispersion at high nanoparticle content. The improved mechanical properties of the adhesive itself are beneficial for the LSS results. As shown in Figure 1(u), compared to the 9.0 MPa of LSS for the control sample, the adhesives with FS obtained values of 13.3 MPa, 17.7 MPa, 17.8 MPa, and 17.4 MPa for 2 wt.%, 5 wt.%, 7 wt.%, and 10 wt.% samples, respectively, which were 48%, 97%, 98%, and 93% higher than the control. The ABL-FS adhesive with 7 wt.% and 10 wt.% FS loading gave a similar LSS as the 5 wt.% sample, even though their tensile strengths were lower than the value of the 5 wt.% sample. The reason is that the LSS can be affected by multiple parameters, such as adhesive tensile strength, toughness, and surface chemistry. Shown in Figure S5 (b), the toughness of the 7 wt.% and 10 wt.% samples exhibited an 85% and 81% improvement compared to the 5 wt.% sample. As proved by the simulation results, rigid particles impede crack propagation and help improve fracture energy,[34, 35] which is reflected in Figure S6 (a) where the failure displacement of single lap shear test was increased with the incorporation of FS. This can also result in the rise of LSS for the ABL-FS adhesive. The difference that existed between the calculated and tested results could come from the interfacial interactions and dispersion status of reinforcing fillers, which were not explicitly modeled. Perfect bonding was assumed here and the damage of ABL and ABL/particle interface was not accounted for in the modeling. And more importantly, the size of the RVE is not large enough in this study to allow for the full development of energy dissipation in ABL-FS composites. In future studies, we will target enhancing our micromechanics-based RVE model to determine the ideal concentration of various nanoparticles that will yield optimal mechanical properties for the ABL-based composites.

For Peer Review

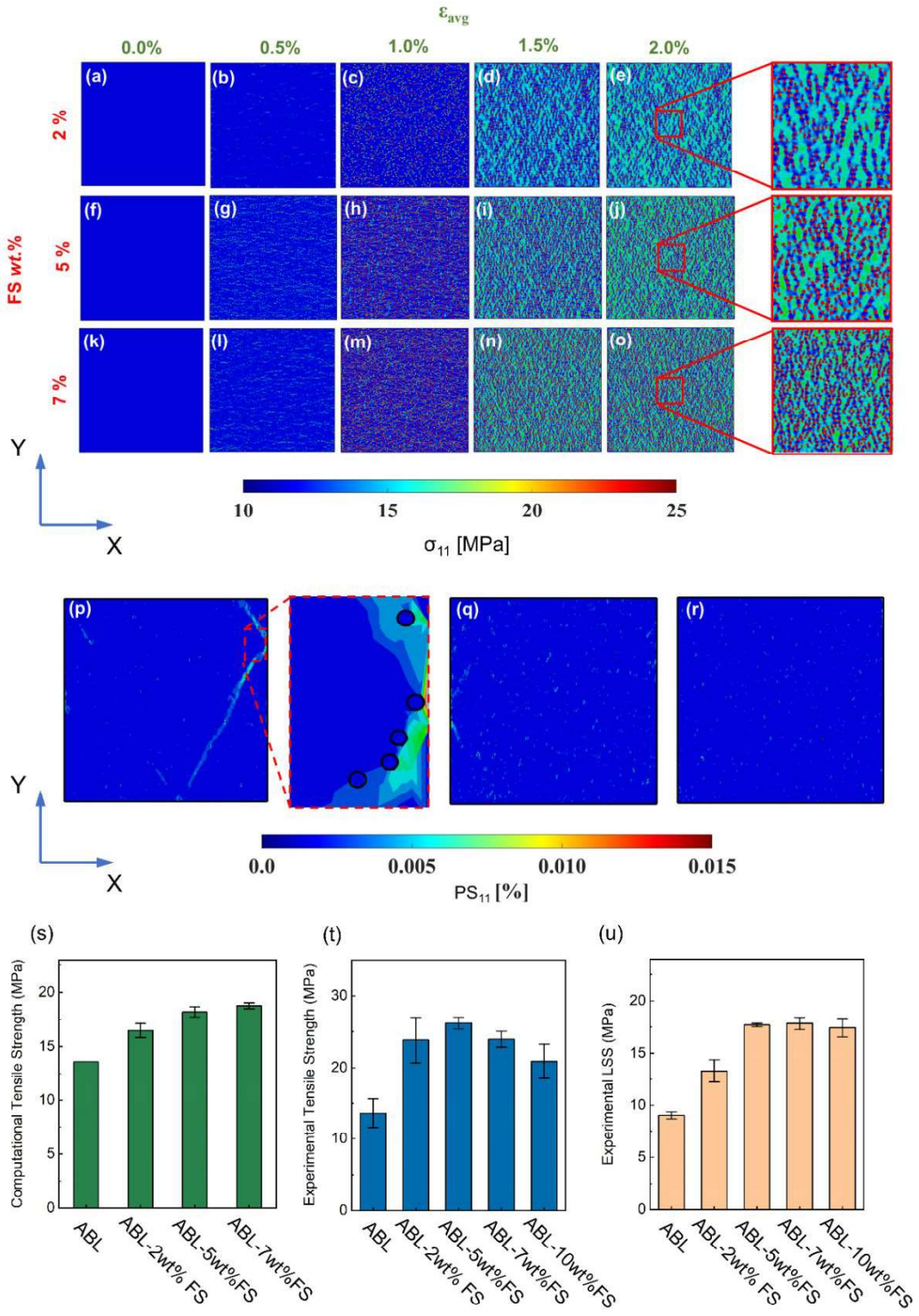

FIGURE 1. (a)-(e), (f)-(j), and (k)-(o) show the σ_{11} distribution at different level of ε_{avg} within 2, 5, and 7 *wt.*% FS-contained composites, respectively; (p)-(r) depict the PS_{11} distribution within the RVEs with 2, 5, and 7 wt.% FS, respectively, at their peak stress (the load was applied in the X direction); (s) summarize computational peak stress; (t)-(u) show the experimental tensile strength and LSS for ABL-based adhesives, respectively.

Because of the high stiffness of the EGS (~86.8 GPa tensile modulus[36, 37]) and its available surface functionality, the EGS was incorporated into the ABL-FS system to modify its mechanical properties and surface energy. The EGS were not considered in the computational study due to their larger size (~2,500 times larger than the FS nanoparticles), which would require a larger RVE volume to accurately represent the microstructure of the ABL-FS-EGS composites. The need for a larger RVE volume to incorporate the statistically considerable number of EGS would also result in an exponential increase in the number of FS nanoparticles that must be included, making the computational study more intensive. So, the reinforcing effect of EGS was analyzed directly through the experimental results and summarized in Figure 2. The LSS consistently increased with increasing loading of EGS and reached a peak of 20.5 MPa at 30 wt.%, which was 16% elevated compared to the control sample (ABL-5 wt.% FS). When the EGS content was raised to 45 wt.%, there was a sharp drop in LSS. This drop in LSS was due to a lack of sufficient ABL matrix to maintain the elasticity and adhesion of the adhesives. The tensile strength (Figure 2(a)) proved that the EGS provided the reinforcement at relatively high loadings. The adhesives with 45 wt.% EGS exhibited a tensile strength of 34.5 MPa compared to 26.2 MPa of the control sample. However, its brittleness caused by high filler loadings led to a low LSS result.

The stress-stain curves of the ABL-FS-EGS adhesive films were summarized in Figure S5(c) and the toughness for these samples was calculated. We found that the addition of the EGS increased the toughness by 560%, 174%, and 5% at the loading of 5 wt.%, 15 wt.% and 30 wt.%. Very high loading of micrometer sized EGS filler is not as effective in matrix reinforcing as nanofillers. The improved matrix toughness caused by filler loading can be attributed to two aspects: (1) improved dispersion of fillers and lignin during mixing and (2) resistance to crack propagation of matrix caused by particulate fillers.

For Peer Review

First, the micrometer sized glass spheres (EGS) help milling of the ABL-FS composite, which further improved the dispersion of lignin and FS particles. As reflected in Figure S4 (SEM images for fractured surfaces of adhesives), the ABL-FS-EGS shows smooth surface without any agglomerates. The finer dispersion could better resist the crack growth (fewer defects in the matrix) and led to higher toughness. Secondly, detachment of the polymer matrix from the glass spheres has to happen during the tensile testing for cracks to grow. Chemical bonding between spheres and the matrix resists such separation. These mechanisms contribute to the improvement of the matrix toughness.[38] The final lap-shear strength (LSS) is a result of compounded effects of both toughness and stiffness enhancement of the matrix. The improvements in the toughness contributed to the final enhancement of LSS. However, consciously adding micrometer size, stiff EGS particles into the polymer matrix led to the brittleness of the composite, causing the drop of toughness (see Figure S5d).[39, 40] Another impact of the use of EGS is its surface functionalities, which could improve the interactions between the adhesive layer and substrate. Shown in Figure S8, the ABL-FS-EGS composite which had the highest surface energy gave the best LSS result.

To compare the adhesion performance of the best ABL-FS-EGS adhesive with the commercial product, an epoxy adhesive (XP0012-YL230) from L&L products was used to prepare the SLS test samples following the same procedure as ABL adhesives. The bonded aluminum joints were kept at 175 ºC for 25 min in the hydraulic carver press for full curing and the LSS was 23.4 MPa (shown in Figure S7). It is intriguing that the thermoplastic ABL adhesive can reach around 90% of the performance of a commercial epoxy-based adhesive, which suggests a great potential for this newly developed adhesive in near future.

For Peer Review

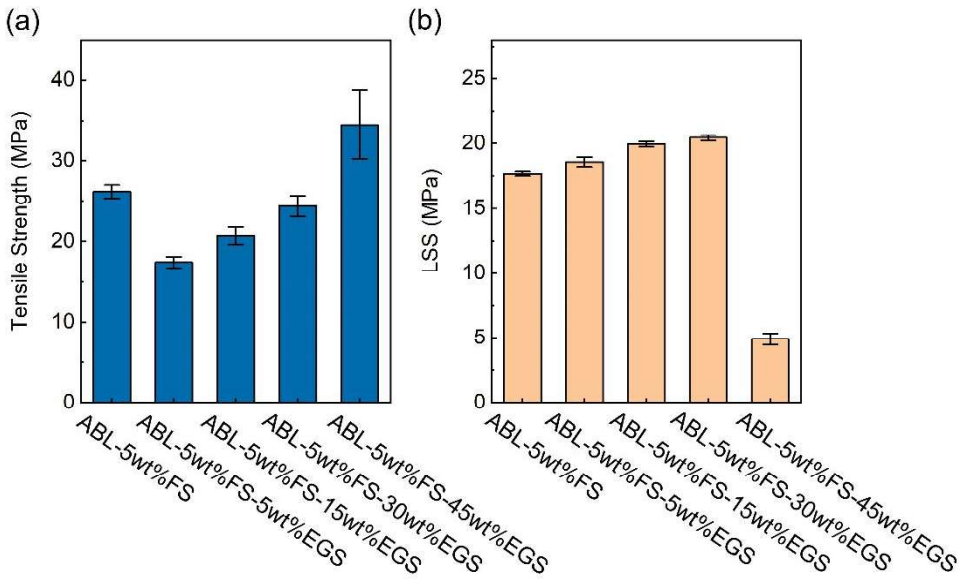

FIGURE 2. The experimental tensile and adhesion properties of ABL-FS-EGS adhesives: (a) tensile strength; (b) LSS results .

3.2 Surface chemistry analysis

The interfacial property between the adhesive and substrate is another important factor that can affect joint strength. The polar functional groups from the reinforcing fillers can improve the interaction between the adhesive and aluminum adherent. The surface chemistry of the ABL-based adhesives were analyzed through FTIR and surface energy measurements to investigate the effect of different fillers. The FTIR results are summarized in Figure 3 to compare the ABL adhesive with different types and loadings of fillers. For the ABL-FS adhesives, shown in Figure 3(a), two sharp peaks at the 2929 cm^{-1} and 2855 cm^{-1} belong to the C-H stretching of the -CH_2 group from the ABL matrix. The peak that appeared at 2238 cm^{-1} was the characteristic peak for NBR, which was attributed to the stretching of -CN groups.[41] The peaks at 1110 cm^{-1} and 970 cm^{-1} belong to Si-O-Si and Si-OH.[41] With a higher loading of FS, the intensity of these two peaks also increased. Adding additional EGS into the ABL-FS adhesive led to an intensity increase in the 910 cm^{-1} peak

(Figure 3(b)), which represented the -C-O- from the epoxide group. The polar functional groups, such as Si-OH and epoxide, increase the dipole moment, which can interact with numerous polar groups and enhance the intermolecular associative force via dipole-dipole interactions. Further, the polar functional groups might form the hydrogen bonds with the aluminum surface to enhance the adhesion strength.[42] Figure S8 summarizes the surface energy for ABL-based adhesives. With the incorporation of FS and EGS, the total energy and polar component went up with the increased loading of fillers for most composites. Among them, the composites with a 30 wt.% content of EGS had the highest total energy, which was 10.5% higher than the control ABL-5 wt.% FS sample. The polar component also presented a 37.3% enhancement. However, continued addition of the EGS leads to a drop in surface energy which could be attributed to a significant loss in the content of the ABL matrix. The same trend was also observed in the LSS results. The modified surface chemistry and improved mechanical properties combined to contribute to the better LSS results of ABL adhesives with fillers.

The fractured interfaces of all the ABL-based adhesives after the lap shear tests are displayed in Figure S9. Even though additional functional groups were incorporated into the ABL matrix and surface energy was improved, all the samples still showed adhesive failure (failure at the interface between substrate and adhesive), which meant that surface treatment, either on adhesive or substrate, could be applied to further improve the performance of ABL-based adhesive bonding.

For Peer Review

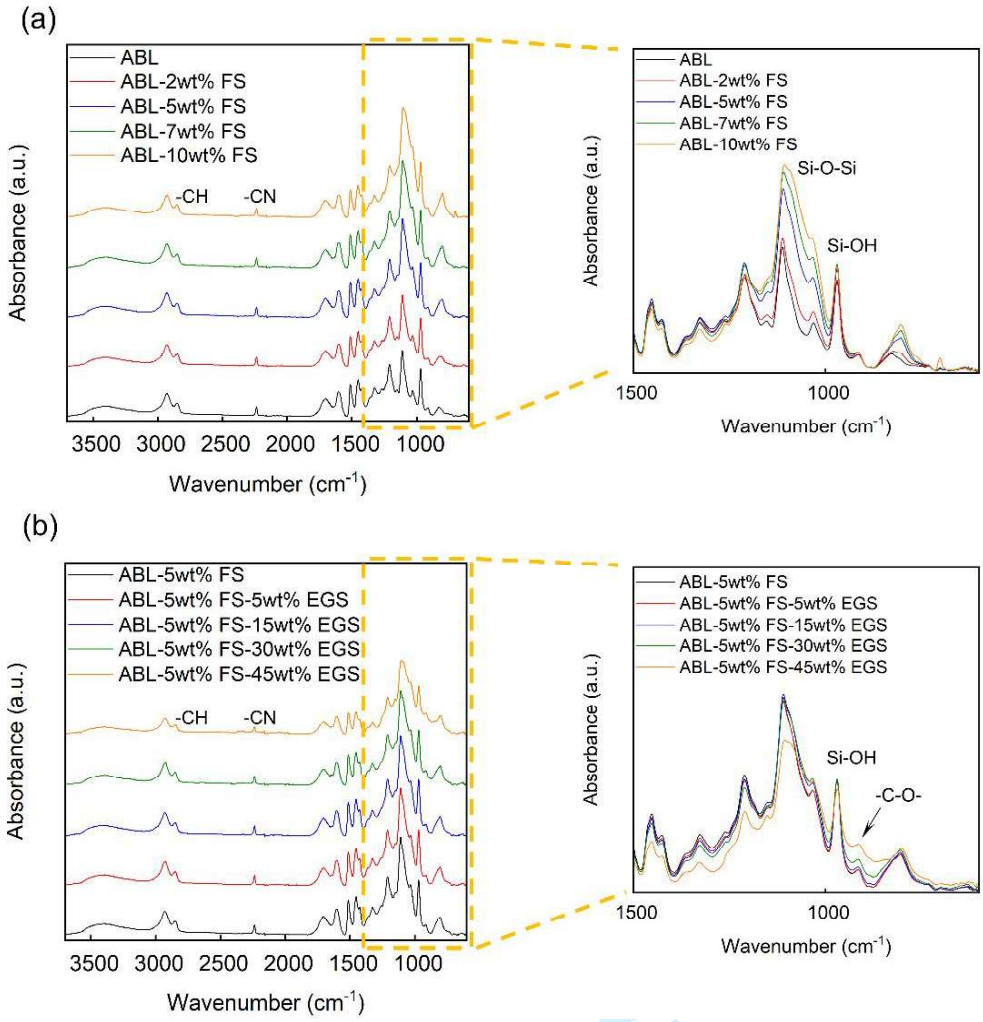

FIGURE 3. The FTIR results for ABL adhesives: (a) ABL-FS; and (b) ABL-FS-EGS adhesives.

3.3 Viscoelastic properties

The tension, compression and shear stresses are usually introduced into metal-metal connecting parts during the joining process. Traditional paste adhesive can be squeezed-out which deteriorates the joint strength. The film adhesive developed within this work with proper rheological properties is designed to address this problem. To evaluate the processability of ABL-based adhesives for joining processes, the viscoelastic properties are included in Figure 4. Since the SLS samples were prepared at a temperature of 160 ºC, the rheological properties of the molten compositions were

investigated at the same temperature. It may be noted that FS particles are generally used as thickening agents.[43] With the incorporation of FS into the ABL matrix, the increased viscosity of the composite could enhance the dispersion and shear-induced separation of the hydrogen-bonded lignin aggregates during the Brabender mixing process. At low concentrations of FS, the dilution effect dominates, and modified morphology leads to a drop in viscosity and storage modulus as shown in Figure 4 (a) and Figure S10 (a). The glass spheres offer a weak reinforcing effect on melt rheology with a low filler concentration. This is a widely accepted topic and investigated as Mullin's effect[44] in filled rubber system. At low concentration of fillers, desorbed, unentangled polymer chains from filler surface show stress softening effect. This is expected to be more prominent with large size of the filler spheres that offer unpacked regions between the fillers and matrix materials. Continued addition of the FS into the ABL matrix, due to the large surface area of nanoparticles and the hydrogen bonds formed between the fillers and matrix resulted in the raised viscosity and storage modulus. Because of the high specific surface area, the FS fillers form aggregate which gradually disperse under an applied shear during the melt-mixing process to form three-dimensional assembly of networks in the polymer matrix.[45] As a result, the viscosity and dynamic mechanical properties of the ABL-FS composites could be a combined effect of the thickening effect of nanoparticles, hydrogen bonding between fillers and matrix, and the dispersion status of additives.

Figure 4 (c) shows the tan δ of all the ABL-FS-based adhesives. The damping factor tan δ is a measure of the ratio of loss to storage moduli (G"/G') of the specimen at a given temperature. The tan δ peak position corresponds to the compositions' glass transition temperature (T_g). Compared to the control sample (41 ºC), all the ABL-FS samples had increased values of T_g, 45 ºC, 52 ºC, 45 ºC, and 53 ºC for 2 wt.%, 5 wt.%, 7 wt.%, and 10 wt.% FS loaded samples, respectively. The

John Wiley & Sons

For Peer Review

rise of T_g was evidence of better interaction between fillers and polymer matrix, and the results agreed well with the improved tensile strength. The magnitude of the tan δ peak represents the dissipation of energy attributed to the internal friction and molecular motions.[42] The damping behavior is affected by the addition of FS nanoparticles, due to the immobilization or confinement of NBR polymer chains by nanofillers. When the FS loading was higher than 2 wt.%, the height of tan δ peak decreased along with the increase of filler content, which indicated the enhanced elastic properties of ABL-FS composites. This is important for certain metal joining processes, such as riveting, to preserve the adhesive between the substrates. For the hybrid joint fabrication with this thermoplastic adhesive, pre-heating the adhesive film above the T_g is helpful, which can decrease the brittleness and improve the processability. Also, specific metal joining method can bring in additional heat that will further soften the adhesive material. To avoid the 'squeeze-out' effect, the viscosity and elastic properties of an adhesive are important, especially at temperatures above the T_g. The incorporation of FS nanoparticles improved the dispersion of lignin particles, and their surface hydroxyl groups were beneficial for higher interfacial adhesion with polymer chains or lignin particles. The higher storage modulus and reduced mobility of polymer segments near the interface[46, 47] of the ABL-FS adhesive favor hybrid joints. Because of the stiffness of the EGS (~86.8 GPa tensile modulus[36]) and the surface functional groups, it was used to enhance the mechanical properties and surface energy of ABL-based adhesives. As shown in Figure S10(b) and Figure 4(b), the introduction of EGS led to an increase of both storage modulus and viscosity.[48] But, as reflected in Figure 4 (b), all the adhesives still possessed the shear thinning effect which would be beneficial for processing.

Figure 4 (d) summarizes the tan δ for all the ABL-FS-EGS-based adhesives. The epoxy groups on the glass sphere surfaces are beneficial for the interfacial interaction between the fillers and

For Peer Review

ABL-FS matrix. By incorporation of stiff EGS, the T_g was increased by 2 ºC, 3 ºC, and 20 ºC with a 15 wt.%, 30 wt.%, and 45 wt.% filler loadings, respectively. However, the composite with 5 wt.% EGS showed a 6 ºC decrease of T_g and its storage modulus was also lower than the control sample. This indicates that at low volume fraction, EGS has a softening effect. The desorbed or unbound, unentangled polymer chains around filler surface show stress softening effect. The existence of voids between the large filler particles and polymer matrix shown in Figure S11, suggests weaker interface at low EGS loading. With further addition of EGS, the matrix stiffening effect increases due to increased volume fraction of immobilized polymer chain on the filler surface. Nonetheless, a clear contrast in the storage moduli of 15 wt.% or higher filler filled ABL compared to the control unfilled ABL could be observed. As the concentration of EGS in the composites grew, the mobility of the polymer chains was further restricted by the fillers.[49, 50] Because of this interaction, ABL with higher EGS content behaved more like an elastic solid, resulting in a higher storage modulus.

For Peer Review

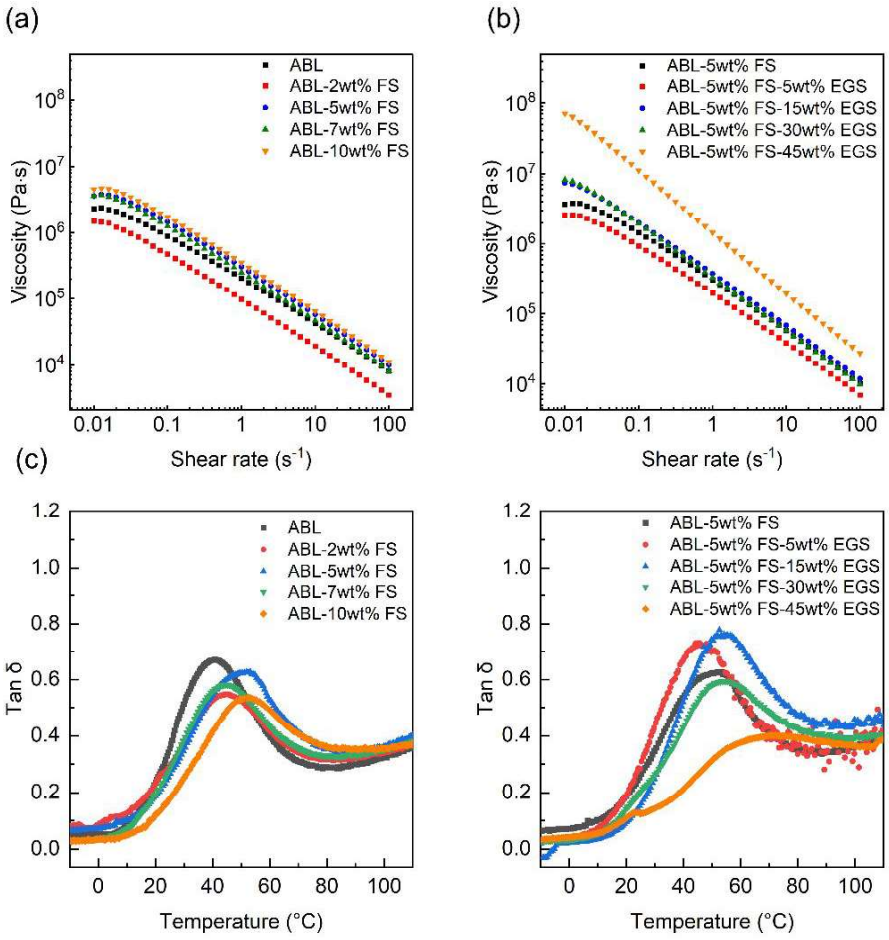

FIGURE 4. Rheological and dynamic-mechanical properties of ABL-based adhesives: (a) complex viscosities of ABL-FS adhesives (160 °C); (b) complex viscosities of ABL-FS-EGS adhesives (160 °C); (c) mechanical damping factor (tan δ) of ABL-FS adhesives; (d) mechanical damping factor (tan δ) of ABL-FS-EGS adhesives.

4. CONCLUSIONS

Sustainable, toughened thermoplastic ABL-based adhesives were developed and characterized in this report. The FS and EGS particulate fillers were used as reinforcing fillers to further improve the LSS values for the ABL-based adhesives because of their good mechanical properties, thickening effect, and surface energies. Various amounts of FS were first incorporated into the ABL matrix to modify the mechanical and viscoelastic properties, as well as the surface chemistry of the adhesives. Because of the large surface area and hydrogen bonding formed with the matrix,

introducing FS increased the viscosity and storage modulus of the ABL-FS adhesive. The higher viscosity of the composites led to a larger shear force during the melt-blending process, which was beneficial for the separation and dispersion of aggregated lignin. The RVE modeling reuslts demonstrated that the stiff FS nanoparticles in the ABL matrix create a torturous pathway for the crack propogation. As a result, the LSS obtained a ~97% improvement with a 5 wt.% FS loading. EGS was added as an additional filler to the ABL-FS composites during a melt-shear-mixing process. Attributed to the intrinsic high stiffness (~86.8 GPa tensile modulus) and surface functionalities of EGS, both storage modulus and viscosity were elevated with increased filler loading. The T_g was further imporved by 20 ºC with a introduction of 45 wt.% of EGS compared to the ABL-FS control sample. With an optimal 30 wt.% EGS in the ABL-FS matrix, the LSS reached 20.5 MPa, which was 16% higher than the ABL-5 wt.% FS sample and reached 90% performance of a commercial epoxy-based adhesive. The fractured interfaces confirmed that the current lap shear test failure was due to the interfacial failure, highlighting that surface treatments such as a plasma or chemical functionalization could further improve adhesion performance. This sustainable thermoplastic adhesive can be applied in the high volume automotive body part assembly. These partly renewable adhesives may be used to replace mechanical fasteners to reduce energy consumption, simplify the manufacturing process for joining of parts, and promote sustainability in the automotive industry.

DECLARATION OF COMPETING INTEREST

The authors declare the following financial interests/personal relationships which may be considered as potential competing interests: Amit K. Naskar reports financial support was provided by US Department of Energy. Naskar, Bowland, Kanbargi, and Yu have filed a provisional patent (application no. 63/409,857, assignee UT-Battelle, LLC).

For Peer Review

ACKNOWLEDGEMENT

This research is supported by Sustainable Transportation Program of the US Department of Energy, Office of Energy Efficiency and Renewable Energy, Vehicle Technologies Office (EERE-VTO). A.K.N. acknlowledges support from the U.S. Department of Energy, Office of Science, Basic Energy Sciences, Materials Sciences and Engineering Division [FWP# ERKCK60] for rheology and DMA data analysis of ABL compositions filled with epoxy-functionalized glass sphreres.

SUPPORTING INFORMATION

Schematic illustration of single-lap shear sample preparation; Details of RVE Modeling; Stress-strain curve for ABL film; SEM images for cryogenically fractured surfaces of selected adhesives; The mechanical properties of ABL adhesives; Surface energy for ABL-based composites; Fractured surfaces of the ABL adhesives, and rheological and dynamic-mechanical properties of ABL-based adhesives. The microstructure of selected adhesives.

DATA AVAILABILITY

The data that support the findings of this study are available from the corresponding author upon reasonable request.

REFERENCES

1. Maggiore S, Banea MD, Stagnaro P, Luciano G. A Review of Structural Adhesive Joints in Hybrid Joining Processes. *Polymers-Basel* 2021;*13*(22):3961.doi: 10.3390/polym13223961.
2. Li WC, Palardy G. Investigation of welding repair methods for thermoplastic composite joints. *Compos Part B-Eng* 2023;*264*:110924.doi: 10.1016/j.compositesb.2023.110924.
3. Wang L, Kelly PV, Ozveren N, et al. Multifunctional polymer composite coatings and adhesives by incorporating cellulose nanomaterials. *Matter* 2022;*6*(2):344-372.doi: 10.1016/j.matt.2022.11.024.
4. Song QB, Li JH, Zeng XL. Minimizing the increasing solid waste through zero waste strategy. *J Clean Prod* 2015;*104*:199-210.doi: 10.1016/j.jclepro.2014.08.027.
5. Sierra-Romero A, Novakovic K, Geoghegan M. Adhesive Interfaces toward a Zero-Waste Industry. *Langmuir* 2022;*38*(50):15476-15493.doi: 10.1021/acs.langmuir.2c02436.

For Peer Review

6. Cui MM, Nguyen NA, Bonnesen PV, et al. Rigid Oligomer from Lignin in Designing of Tough, Self-Healing Elastomers. *Acs Macro Lett* 2018;*7*(11):1328-1332.doi: 10.1021/acsmacrolett.8b00600.
7. Tran CD, Chen JH, Keum JK, Naskar AK. A New Class of Renewable Thermoplastics with Extraordinary Performance from Nanostructured Lignin-Elastomers. *Adv Funct Mater* 2016;*26*(16):2677-2685.doi: 10.1002/adfm.201504990.
8. Gao SS, Cheng ZH, Zhou X, et al. Fabrication of lignin based renewable dynamic networks and its applications as self -healing, antifungal and conductive adhesives. *Chem Eng J* 2020;*394*:124896.doi: 10.1016/j.cej.2020.124896.
9. Sutton JT, Rajan K, Harper DP, Chmely SC. Improving UV Curing in Organosolv Lignin-Containing Photopolymers for Stereolithography by Reduction and Acylation. *Polymers-Basel* 2021;*13*(20):3473.doi: 10.3390/polym13203473.
10. Liao JJ, Abd Latif NH, Trache D, Brosse N, Hussin MH. Current advancement on the isolation, characterization and application of lignin. *Int J Biol Macromol* 2020;*162*:985-1024.doi: 10.1016/j.ijbiomac.2020.06.168.
11. Choi JH, Jang SK, Kim JH, et al. Simultaneous production of glucose, furfural, and ethanol organosolv lignin for total utilization of high recalcitrant biomass by organosolv pretreatment. *Renew Energ* 2019;*130*:952-960.doi: 10.1016/j.renene.2018.05.052.
12. Peng ZY, Zou YB, Xu SQ, Zhong WB, Yang WT. High-Performance Biomass-Based Flexible Solid-State Supercapacitor Constructed of Pressure-Sensitive Lignin-Based and Cellulose Hydrogels. *Acs Appl Mater Inter* 2018;*10*(26):22190-22200.doi: 10.1021/acsami.8b05171.
13. Vaidya AA, Collet C, Gaugler M, Lloyd-Jones G. Integrating softwood biorefinery lignin into polyhydroxybutyrate composites and application in 3D printing. *Mater Today Commun* 2019;*19*:286-296.doi: 10.1016/j.mtcomm.2019.02.008.
14. Moreno A, Morsali M, Sipponen MH. Catalyst-Free Synthesis of Lignin Vitrimers with Tunable Mechanical Properties: Circular Polymers and Recoverable Adhesives. *Acs Appl Mater Inter* 2021;*13*(48):57952-57961.doi: 10.1021/acsami.1c17412.
15. van de Velde N, Javornik S, Sever T, et al. Bio-Based Epoxy Adhesives with Lignin-Based Aromatic Monophenols Replacing Bisphenol A. *Polymers-Basel* 2021;*13*(22):3879.doi: 10.3390/polym13223879.
16. Rahman MM, Netravali AN, Tiimob BJ, Apalangya V, Rangari VK. Bio-inspired " green" nanocomposite using hydroxyapatite synthesized from eggshell waste and soy protein. *Journal of Applied Polymer Science* 2016;*133*(22):43477.doi: 10.1002/app.43477.
17. Amini A, Fallah A, Sedaghat A, et al. Natural vs. Synthetic Phosphate as Efficient Heterogeneous Compounds for Synthesis of Quinoxalines. *Int J Mol Sci* 2021;*22*(24):13665.doi: 10.3390/ijms222413665.
18. Fazli A, Rodrigue D. Waste Rubber Recycling: A Review on the Evolution and Properties of Thermoplastic Elastomers. *Materials* 2020;*13*(3):782.doi: 10.3390/ma13030782.
19. Simmons KL, Kuang W, Burton SD, et al. H-Mat hydrogen compatibility of polymers and elastomers. *Int J Hydrogen Energ* 2021;*46*(23):12300-12310.doi: 10.1016/j.ijhydene.2020.06.218.
20. Pradhan B, Srivastava SK. Synergistic effect of three-dimensional multi-walled carbon nanotube-graphene nanofiller in enhancing the mechanical and thermal properties of high-performance silicone rubber. *Polym Int* 2014;*63*(7):1219-1228.doi: 10.1002/pi.4627.

21. Ponnamma D, Sadasivuni KK, Strankowski M, Guo QP, Thomas S. Synergistic effect of multi walled carbon nanotubes and reduced graphene oxides in natural rubber for sensing application. *Soft Matter* 2013;*9*(43):10343-10353.doi: 10.1039/c3sm51978c.
22. Dominic CDM, Joseph R, Begum PMS, et al. Chitin nanowhiskers from shrimp shell waste as green filler in acrylonitrile-butadiene rubber: Processing and performance properties. *Carbohyd Polym* 2020;*245*:116505.doi: 10.1016/j.carbpol.2020.116505.
23. Guo YB, Cao ZQ, Wang DG, Liu SH. Improving the friction and abrasion properties of nitrile rubber hybrid with hollow glass beads. *Tribol Int* 2016;*101*:122-130.doi: 10.1016/j.triboint.2016.04.022.
24. Kuznetsov A, Kumar G, Ardagh MA, et al. On the Economics and Process Design of Renewable Butadiene from Biomass-Derived Furfural. *Acs Sustain Chem Eng* 2020;*8*(8):3273-3282.doi: 10.1021/acssuschemeng.9b06881.
25. Karp EM, Eaton TR, Nogue VSI, et al. Renewable acrylonitrile production. *Science* 2017;*358*(6368):1307-1310.doi: 10.1126/science.aan1059.
26. Kanbargi N, Hoskins D, Gupta S, et al. A renewable lignin-based thermoplastic adhesive for steel joining. *Eur Polym J* 2023;*189*:111981.doi: 10.1016/j.eurpolymj.2023.111981.
27. Antonino LD, Garcia GES, Gouveia JR, et al. Polyurethane adhesives from castor oil and modified lignin via reaction with propylene carbonate. *Journal of Applied Polymer Science* 2022;*139*(27):e52477.doi: 10.1002/app.52477.
28. Vattathurvalappil SH, Haq M. Thermomechanical characterization of Nano-Fe_3O_4 reinforced thermoplastic adhesives and single lap-joints. *Compos Part B-Eng* 2019;*175*:107162.doi: doi.org/10.1016/j.compositesb.2019.107162.
29. Xu CC, Ramani K, Kumar G. Thermoplastic adhesive bonding of galvanized steel to polypropylene composite and its durability. *Int J Adhes Adhes* 2002;*22*(3):187-195.doi: doi.org/10.1016/S0143-7496(01)00054-9.
30. Kadiyala AK, Bijwe J. Investigations on performance and failure mechanisms of high temperature thermoplastic polymers as adhesives. *Int J Adhes Adhes* 2016;*70*:90-101.doi: 10.1016/j.ijadhadh.2016.05.011.
31. Shin Y, Qiao Y, Canfield N, et al. Significant slowdown of plasma-optimized surface energy deactivation by vacuum sealing for efficient adhesive bonding. *Compos Part B-Eng* 2022;*240*:110001.doi: 10.1016/j.compositesb.2022.110001.
32. Mohammadpour E, Awang M, Kakooei S, Akil HM. Modeling the tensile stress-strain response of carbon nanotube/polypropylene nanocomposites using nonlinear representative volume element. *Mater Design* 2014;*58*:36-42.doi: 10.1016/j.matdes.2014.01.007.
33. Kari S, Berger H, Rodriguez-Ramos R, Gabbert U. Computational evaluation of effective material properties of composites reinforced by randomly distributed spherical particles. *Compos Struct* 2007;*77*(2):223-231.doi: 10.1016/j.compstruct.2005.07.003.
34. Kalaitzidou K, Fukushima H, Drzal LT. Mechanical properties and morphological characterization of exfoliated graphite-polypropylene nanocomposites. *Compos Part a-Appl S* 2007;*38*(7):1675-1682.doi: 10.1016/j.compositesa.2007.02.003.
35. Yu ZY, Drzal LT. Functionalized graphene oxide as coupling agent for graphene nanoplatelet/epoxy composites. *Polym Composite* 2020;*41*(3):920-929.doi: 10.1002/pc.25423.
36. Potters. *"Spheriglass Product Overview"*. https://www.pottersindustries.com/micro-glass-beads/ (Accessed on January 31st, 2023).

For Peer Review

37. Spoerk M, Savandaiah C, Arbeiter F, Sapkota J, Holzer C. Optimization of mechanical properties of glass-spheres-filled polypropylene composites for extrusion-based additive manufacturing. *Polym Composite* 2019;*40*(2):638-651.doi: 10.1002/pc.24701.
38. Chandrasekaran S, Sato N, Tölle F, et al. Fracture toughness and failure mechanism of graphene based epoxy composites. *Compos Sci Technol* 2014;*97*:90-99.doi: 10.1016/j.compscitech.2014.03.014.
39. Fu SY, Feng XQ, Lauke B, Mai YW. Effects of particle size, particle/matrix interface adhesion and particle loading on mechanical properties of particulate-polymer composites. *Compos Part B-Eng* 2008;*39*(6):933-961.doi: 10.1016/j.compositesb.2008.01.002.
40. Quazi RT, Bhattacharya SN, Kosior E. The effect of dispersed paint particles on the mechanical properties of rubber toughened polypropylene composites. *J Mater Sci* 1999;*34*(3):607-614.doi: Doi 10.1023/A:1004515300637.
41. Hait S, Valentin JL, Jimenez AG, et al. Poly(acrylonitrile-co-butadiene) as polymeric crosslinking accelerator for sulphur network formation. *Heliyon* 2020;*6*(8):e04659.doi: 10.1016/j.heliyon.2020.e04659.
42. Wei HY, Xia J, Zhou WL, et al. Adhesion and cohesion of epoxy-based industrial composite coatings. *Compos Part B-Eng* 2020;*193*(15):108035.doi: 10.1016/j.compositesb.2020.108035.
43. Alaee P, Kamkar M, Arjmand M. Fumed Silica-Based Suspensions for Shear Thickening Applications: A Full-Scale Rheological Study. *Langmuir* 2022;*38*(16):5006-5019.doi: 10.1021/acs.langmuir.2c00591.
44. Diani J, Fayolle B, Gilormini P. A review on the Mullins effect. *Eur Polym J* 2009;*45*(3):601-612.doi: 10.1016/j.eurpolymj.2008.11.017.
45. Cassagnau P. Melt rheology of organoclay and fumed silica nanocomposites. *Polymer* 2008;*49*(9):2183-2196.doi: 10.1016/j.polymer.2007.12.035.
46. Omrani A, Simon LC, Rostami AA. The effects of alumina nanoparticle on the properties of an epoxy resin system. *Mater Chem Phys* 2009;*114*(1):145-150.doi: 10.1016/j.matchemphys.2008.08.090.
47. Sunny AT, Vijayan PP, Adhikari R, Mathew S, Thomas S. Copper oxide nanoparticles in an epoxy network: microstructure, chain confinement and mechanical behaviour. *Phys Chem Chem Phys* 2016;*18*(29):19655-19667.doi: 10.1039/c6cp02361d.
48. Reynolds JP, Rau DA, Williams CB, Bortner MJ. A rheological method to predict printability of high solids content inks via ultraviolet-assisted material extrusion. *Addit Manuf* 2023;*75*:103745.doi: 10.1016/j.addma.2023.103745.
49. Gogoi R, Kumar N, Mireja S, et al. Effect of Hollow Glass Microspheres on the Morphology, Rheology and Crystallinity of Short Bamboo Fiber-Reinforced Hybrid Polypropylene Composite. *Jom-Us* 2019;*71*(2):548-558.doi: 10.1007/s11837-018-3268-3.
50. Capela C, Ferreira JM, Costa JM, Mendes N. Mechanical Properties of Injection-Molded Glass Microsphere-Reinforced Polyamide. *J Mater Eng Perform* 2016;*25*(10):4256-4265.doi: 10.1007/s11665-016-2237-7.

For Peer Review